JOURNAL OF MAGNETIC RESONANCE **130,** 287–291 (1998)
ARTICLE NO. MN971305

^{14}N NMR Echo in NH_4ClO_4 after the Pulse Sequence $(\theta_1)_x-\tau-(\theta_2)_y-t$

M. Punkkinen, A. H. Vuorimäki, E. E. Ylinen, and A. Kaikkonen

Wihuri Physical Laboratory, Department of Physics, University of Turku, FIN-20014 Turku, Finland

Received April 1, 1997; revised September 8, 1997

We have derived a closed-form expression for the solid echo signal of quadrupolar $I = 1$ nuclei after the pulse sequence $(\theta_1)_x-\tau-(\theta_2)_y-t$ for arbitrary values of the RF nutation frequency $\omega_1 = \gamma B_1$ and the quadrupolar frequency ω_Q. In the case of single crystals both the true echo term of this expression and its induction-signal-like terms are important as shown by experiments on ^{14}N nuclei in NH_4ClO_4 crystal. Conditions for obtaining the maximal echo in powder samples are presented. A very low B_1 field together with long RF pulses may distort even the central part of the spectrum, resulting in strange looking apparent spectra. © 1998 Academic Press

INTRODUCTION

The quadrupolar echo was first proposed and studied by Solomon (*1*). The most commonly used pulse sequence for the observation of the echo is $(\theta_1)_x-\tau-(\theta_2)_y-$t. Here the second pulse is 90° phase shifted relative to the first pulse and follows it after the delay of τ. The echo maximum is observed roughly at the time $t = \tau$ after the second pulse. The method has been widely used for studies of spin–lattice relaxation and NMR spectra of quadrupolar nuclei with the spin $I \geq 1$.

The discovery of multiquantum transitions renewed the interest in quadrupolar nuclei. Vega and Pines (*2*) and Wokaun and Ernst (*3*) presented general methods for solving exactly the signal shape after the two-pulse sequence mentioned above and also after more complicated sequences. Man (*4*) applied these methods to spins $I = \frac{3}{2}$. Bloom *et al.* (*5*) calculated the pure echo term for $I = 1$ nuclei in a closed form and studied the distortion of the spectrum, obtained from the echo via Fourier transform, as functions of the pulse length and the nutation frequency $\omega_1 = \gamma B_1$, where B_1 is the RF magnetic field and γ the gyromagnetic ratio.

Below we present closed-form solutions for the induction signal and also for the echo after the two-pulse sequence mentioned above, when the ratio of ω_1 to the quadrupolar frequency ω_Q is arbitrary. The calculation is done at exact resonance with the frequency of the RF field ω_{RF} equal to γB_0, where $\mathbf{B}_0$ is the static external field. The results are compared with experiments on ^{14}N nuclei in a single crystal of NH_4ClO_4 and in a corresponding polycrystalline sample. In the single crystal also the induction-signal-like terms of the echo are important and their effect is studied in detail. For the polycrystalline sample the conditions which produce the maximum echo amplitude are found. Some manifestations of spectral distortion are also shown.

THEORY

We calculate the free induction and echo signals for $I = 1$ nuclei by using the time-dependent Schrödinger equation. The state of the spin system is described by the wavefunction

$$\Psi = \sum_m c_m \Phi_m, \qquad [1]$$

where the c_m's are the weight factors and the Φ_m's the spin eigenfunctions in the absence of the RF field. The stationary energy levels of a nuclear spin, in the absence of the RF field, are determined by the Hamiltonian (in units of $\hbar$)

$$H = -\gamma B_0 I_z + \omega_Q[3I_z^2 - I^2]/3, \qquad [2]$$

if the nucleus interacts with the static magnetic field $\mathbf{B}_0$ more strongly than with the electric field gradient. The quadrupolar frequency ω_Q is given by

$$\omega_Q = (3\cos^2\theta - 1 + \eta \sin^2\theta \cos 2\phi)3e^2qQ/8\hbar. \qquad [3]$$

Here e^2qQ is the quadrupole coupling constant, η is the asymmetry parameter, and θ and φ are the polar angles of $\mathbf{B}_0$ in the principal axis frame of the quadrupole interaction. The NMR spectrum of $I = 1$ nuclei in single crystals consists of a doublet with the individual lines at $\pm\omega_Q$ relative to the unshifted resonance frequency $\omega_0 = \gamma B_0$.

When a RF pulse (amplitude B_1) is applied parallel to the x axis of the frame rotating at the frequency ω_{RF} about $\mathbf{B}_0$, the Hamiltonian in this frame becomes

$$H = \Delta\omega I_z + \omega_Q[3I_z^2 - I^2]/3 + \omega_1 I_x, \qquad [4]$$

1090-7807/98 $25.00

with $\Delta\omega = \omega_{RF} - \omega_0$ and $\omega_1 = \gamma B_1$. The corresponding time-dependent Schrödinger equation involving the wavefunction ψ leads to the coupled differential equations

$$\frac{d}{dt}\begin{pmatrix} c_{-1} \\ c_0 \\ c_1 \end{pmatrix} = i\begin{pmatrix} -\Delta\omega - \omega_Q/3 & \omega_1/\sqrt{2} & 0 \\ \omega_1/\sqrt{2} & 2\omega_Q/3 & \omega_1/\sqrt{2} \\ 0 & \omega_1/\sqrt{2} & \Delta\omega - \omega_Q/3 \end{pmatrix} \times \begin{pmatrix} c_{-1} \\ c_0 \\ c_1 \end{pmatrix}. \quad [5]$$

These determine the time variation of the weight coefficients c_m. In all our experiments we applied the RF field at the frequency ω_0 which makes $\Delta\omega = 0$. The matrix equation [5] is solved first.

After the $(\theta_1)_x$ pulse the weights c_m have the time dependence $\exp(-iE_m\tau/\hbar)$. The free induction signal amplitude is then calculated from $\langle\Psi|I_+|\Psi\rangle$

$$\mathrm{FID}_y = (N_1 - N_{-1})(\omega_1/R_1)\sin R_1 t_1 \cos[\omega_Q(t_1/2 + \tau)]$$
$$R_1 = [\omega_1^2 + \omega_Q^2/4]^{1/2}. \quad [6]$$

Here N_1 and N_{-1} are the level populations before the application of the pulse and t_1 is the pulse length. The x component of the FID vanishes at exact resonance $\Delta\omega = 0$.

During the second pulse the weights c_m obey an equation similar to Eq. [5] but with $\omega_1/\sqrt{2}$ multiplied by i (on the upper right side of the main diagonal) or by $-i$ (on the lower left side of the main diagonal). When the time dependence $\exp(-iE_m t/\hbar)$ after the second pulse is taken into account, we obtain for the Echo

$$\begin{aligned}\mathrm{Echo}_x = {} & (N_1 - N_{-1})(\omega_1/R_1) \\ & \times \{-\cos\theta_1 \sin\theta_2 \cos[\omega_Q(-t_1/2 + t_2/2 + t)] \\ & + (\omega_Q/2R_2)\sin\theta_1 \sin\theta_2 \\ & \times \sin[\omega_Q(-t_1/2 + t_2/2 + t)]\} \quad [7] \\ \mathrm{Echo}_y = {} & (N_1 - N_{-1})(\omega_1/R_1)\sin\theta_1 \\ & \times \{(\omega_1/R_2)^2 \sin^2\theta_2 \cos[\omega_Q(-t_1/2 - \tau + t)] \\ & + (\cos^2\theta_2 - \omega_Q^2 \sin^2\theta_2/4R_2^2) \\ & \times \cos[\omega_Q(t_1/2 + \tau + t)] \\ & - (\omega_Q/R_2)\sin\theta_2 \cos\theta_2 \\ & \times \sin[\omega_Q(t_1/2 + \tau + t)]\}. \quad [8]\end{aligned}$$

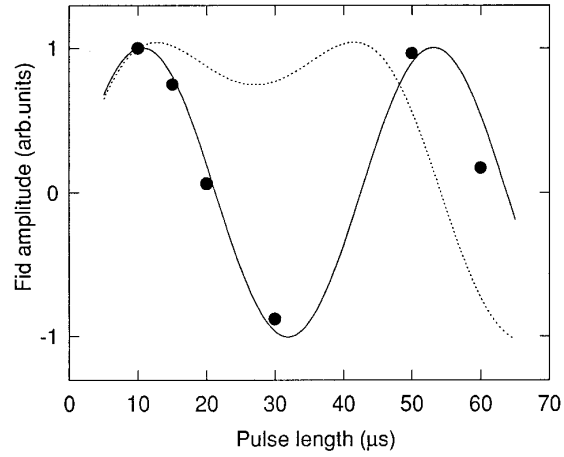

FIG. 1. Induction signal amplitude versus the pulse length: solid curve (Eq. [6]); dotted curve (see text); experimental points for ^{14}N in a NH_4ClO_4 single crystal with $\omega_1 = 136 \times 10^3$ rad/s and $\omega_Q = 116 \times 10^3$ rad/s.

Here t_2 is the length of the second pulse, $\theta_1 = R_1 t_1$, $\theta_2 = R_2 t_2$, and $R_2 = [\omega_1^2 + \omega_Q^2/4]^{1/2}$ during the second pulse.

The results [6]–[8] can be derived also by other methods (*2, 3*). The pure echo term or the first term in [8] is exactly the same as that considered by Bloom *et al.* (*5*). However, they did not consider the remaining two terms since they were interested in powder samples. In such samples the second and the third terms of [8] die out very fast after the second pulse and contribute in practice nothing to the observed echo.

RESULTS AND DISCUSSION

We chose NH_4ClO_4 as our sample since its ^{14}N ($I = 1$) nuclei have a relatively small quadrupole coupling. All the nitrogens are crystallographically equivalent (*6*). The maximum quadrupole frequency at room temperature equals $\nu_{Qmax} = \omega_{Qmax}/2\pi = 40.5$ kHz (*7*), where $\omega_{Qmax} = \omega_Q$ for $\theta = 0^0$ in Eq. [3]. However, there are two sets of differently oriented principal axes of the quadrupole coupling, and thus two doublets are observed by NMR. The spectrometer frequency was kept equal to $\nu_{RF} = \nu_0 = \gamma B_0/2\pi = 11.08$ MHz in all our experiments.

At first we measured the nitrogen spin–lattice relaxation time and obtained the result $T_1 \cong 41$ s at 293 K. Usually the repetition time between successive pulse sequences was 2 min. The RF field was calibrated by the proton NMR from a rubber sample, measured at the same resonance frequency but at a lower field. An independent calibration was obtained from the ^{14}N signal after orientating the NH_4ClO_4 crystal in such a way that one doublet collapsed into a single line. The results of these two methods agreed quite well with each other.

In Fig. 1 the signal amplitude Fid_y of Eq. [6] (with a

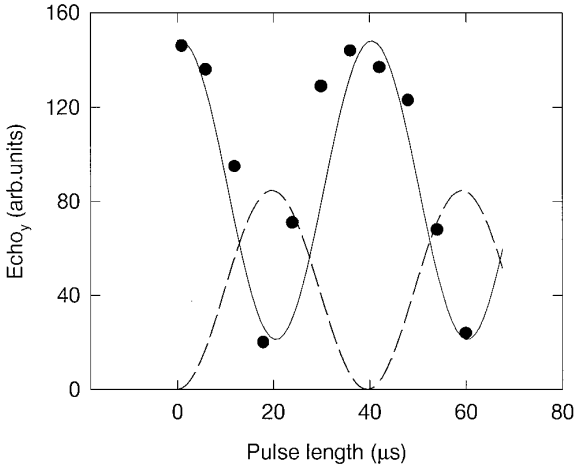

FIG. 2. The echo amplitude at $t = \tau + t_1/2$ versus the length of the second pulse for $\omega_1 = 60.3 \times 10^3$ rad/s, $\omega_Q = 104.2 \times 10^3$ rad/s, and $\tau = 20.2$ μs. The solid curve represents all the three terms of Echo$_y$ in [8], while the dashed curve corresponds to the first term.

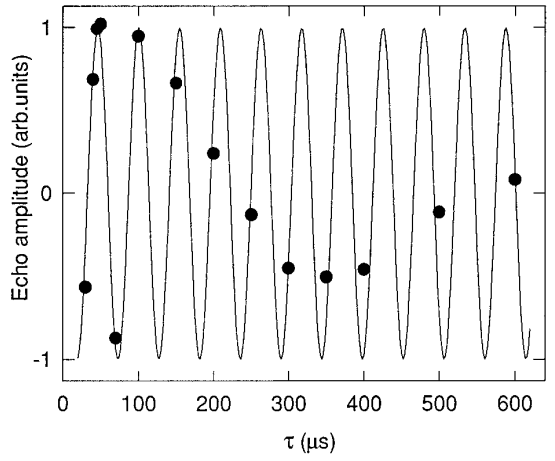

FIG. 3. Signal amplitude at $t = \tau + t_1/2$ after the pulse sequence $(\theta_1)_x-\tau-(\theta_2)_y-t$ versus τ. The solid curve represents the second term of Echo$_y$ in Eq. [8].

constant τ), as a function of the pulse length t_1, is compared with the experimental data for the doublet with $\omega_Q = 116 \times 10^3$ rad/s, when $\omega_1 = 136 \times 10^3$ rad/s. The agreement is satisfactory. The dotted curve representing the function $\sin[\omega_1 t_1(2\sin(\omega_Q t_1/2)/\omega_Q t_1)]$ does not follow the experimental points at all. This function was derived by using the well-known result for the Fourier transform of a short RF pulse (length t_1, amplitude B_1, and frequency ω_0), according to which the pulse amplitude is reduced to $B_1' = 2B_1\sin(\omega_Q t_1/2)/\omega_Q t_1$ at the frequencies $\omega_0 \pm \omega_Q$. The pulse should nutate the magnetization of the nuclei resonating at those frequencies by the angle $\gamma B_1' t_1$, which leads to the signal amplitude $\sin \gamma B_1' t_1$ presented by the dotted curve.

In the echo experiments we used an extended version of the quadrature phase cycling where the phase of the second pulse was switched between y and $-y$. This makes the Echo$_x$ signal vanish while Echo$_y$ remains unaffected. The first term of Echo$_y$ in [8] is the true echo but its second and third terms behave like the free induction signal. The solid curve in Fig. 2 represents these three terms as a function of the length of the second pulse for the doublet with $\omega_Q = 104.2 \times 10^3$ rad/s, when $\omega_1 = 60.3 \times 10^3$ rad/s, $\tau = 20.2$ μs, and $t = \tau + t_1/2 = 30$ μs. Solid circles represent the corresponding experimental amplitudes after the Fourier transform of the echo for our single crystal. The dashed curve represents the true echo or the first term of Eq. [8]. For $t_2 = 39.4$ μs the nutation angle is $\theta_2 = R_2 t_2 = 180°$ and only the second term of Echo$_y$ survives. For $\theta_2 = 90°$ or $t_2 = 19.7$ μs the first two terms contribute. The importance of the second and third terms is clearly seen in the case of a single crystal.

Figure 3 describes an experiment on the NH_4ClO_4 single crystal, where τ was varied in the pulse sequence $(90°)_x-\tau-(180°)_y-t$. Signals were acquired from $t = \tau + t_1/2$ onward and the corresponding Fourier transforms were calculated. Since the signal in such a situation contains exclusively the induction signal component, the spectral area of each resonance should vary with τ according to $\cos \omega_Q[2\tau + t_1]$. Such a behavior is clearly observed, although the theoretical curve oscillates with a constant amplitude since attenuation effects were not included.

In some experiments on powder samples, for example, when studying spin–lattice relaxation, one may be interested to know the condition for the maximum echo amplitude after the two-pulse sequence. In Fig. 4 we have calculated the signal at $t = \tau + t_1/2$ as functions of the apparent flip angles $\omega_1 t_1$ and $\omega_1 t_2$ of the two RF pulses for $\omega_1/\omega_{Qmax} = 0.28$. This ratio was chosen because it was

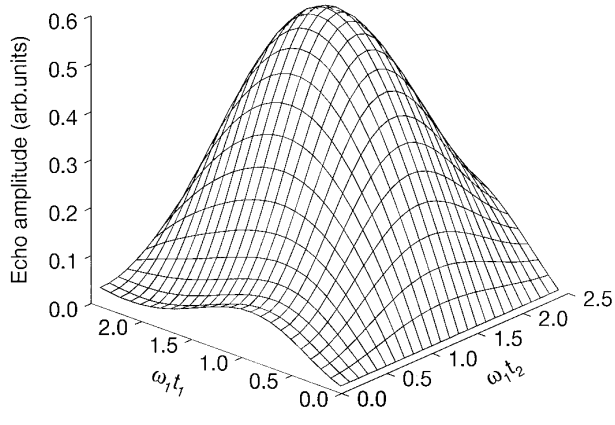

FIG. 4. Echo amplitude at $t = \tau + t_1/2$ as a function of the flip angles $\omega_1 t_1$ and $\omega_1 t_2$ for a powder sample of $I = 1$ nuclei with $\omega_1/\omega_{Qmax} = 0.28$.

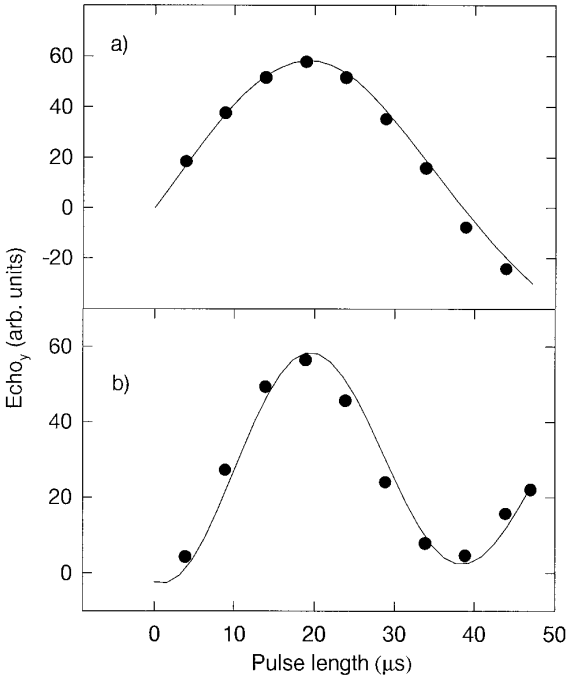

FIG. 5. Cross section of Fig. 4 as functions of t_1 (a) and t_2 (b) together with the corresponding experimental points for ^{14}N in polycrystalline NH_4ClO_4 with $\omega_1/\omega_{Qmax} = 0.28$.

easily obtainable with the Bruker broadband probe. Figures 5a and 5b represent one-dimensional cross sections of Fig. 4 as functions of the pulse lengths t_1 and t_2, together with experimental points.

Often it would be desirable to obtain the true NMR powder spectrum from the true echo or the first term of Echo$_y$ in [8]. A long interval τ between the RF pulses makes the induction-signal-like terms vanish on average so that only the true echo survives. Unfortunately, in the case of identical RF pulses this term contains the multiplier $[\omega_1 t_1 \sin Rt_1/Rt_1]^3$, which is $\omega_1^3 t_1^3$ (or independent of ω_Q) near the center of the resonance or $\omega_Q \ll \omega_1$ but much smaller than $\omega_1^3 t_1^3$ for $\omega_Q \gg \omega_1$. A similar situation is produced even by nonidentical RF pulses. The only way to avoid such a distortion far off from ω_0 is to use pulse lengths with $\omega_{Qmax} t_i < 1$, $i = 1, 2$ (5). For $\omega_1 < \omega_Q$ the signal-to-noise ratio is then drastically reduced. Therefore it is always advantageous to use as intense a B_1 field as possible. Although these distortions are strongest at the wings of the NMR absorption, some caution must be exercised even near the center of the spectrum. Figures 6a and 6b show theoretically computed powder spectra (dashed curves) for two ratios $\omega_1/\omega_{Qmax} = 0.28$ (a) and $\omega_1/\omega_{Qmax} = 0.49$ (b) and the respective pulse lengths 19 and 13 μs. The spectra were obtained from the three terms of Echo$_y$ in [8], calculated for evenly distributed crystal orientations in the external $\mathbf{B}_0$ field, weighted with $\sin\theta$ and then summed up. The echo signal obtained was multiplied with the Gaussian decay function $\exp(-\alpha t^2)$, which has a smoothing effect on the spectrum but does not change its structure. The parameter α was the only fitting parameter (besides the overall scaling factor) and the value $1/\alpha^{1/2} = 158$ μs was chosen to produce the right amplitude for the narrow components near ± 20 kHz in Fig. 6. For the smaller ratio $\omega_1/\omega_{Qmax} = 0.28$ a distortion-related maximum appears at the center of the spectrum, which disappears when ω_1 is increased and pulse lengths are decreased. The spectral wings are strongly suppressed in both cases. The same behavior is observed in the corresponding experimental spectra.

The odd spectral shapes can be understood by considering the transition region from the undistorted to distorted part of the spectrum. For $\omega_1 < \omega_Q$ this corresponds roughly to $Rt_i \cong \omega_Q t_i/2 = 1$, which in the case of identical pulses produces an amplitude reduction of 40%. The conditions of Fig. 6a give for this boundary the result $\omega_Q = 105 \times 10^3$ rad/s, which is really larger than $\omega_1 = 71 \times 10^3$ rad/s. These boundaries fall between the narrow spectral maxima and ω_0, which means that only the very narrow central section of the spectral in Fig. 6a is true. At $\pm\omega_Q$

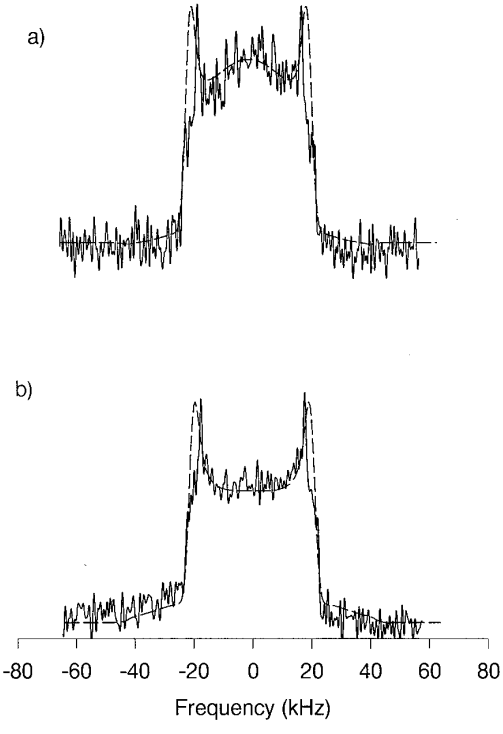

FIG. 6. Experimentally observed powder spectra, obtained from the echo of ^{14}N in polycrystalline NH_4ClO_4, for $\omega_1/\omega_{Qmax} = 0.28$ with $t_1 = t_2 = 19$ μs (a) and for $\omega_1/\omega_{Qmax} = 0.49$ with $t_1 = t_2 = 13$ μs (b). The dashed curves are the corresponding simulated spectra (see text).

relative to ω_0 the spectral amplitude is 40% reduced by distortions and even more at the narrow maxima. In Fig. 6b the boundaries lie outside the narrow maxima and therefore the spectral part between these maxima is practically undistorted.

It should be noticed that even one RF pulse and the subsequent Fourier transform do not usually produce the true absorption spectrum because of the factor $\omega_1 \sin R_1 t_1 / R_1$ in [6]. This distortion, however, is not at all so severe as in the case of the echo.

REFERENCES

1. I. Solomon, *Phys. Rev.* **110,** 61 (1958).
2. S. Vega and A. Pines, *J. Chem. Phys.* **66,** 5624 (1977).
3. A. Wokaun and R. R. Ernst, *J. Chem. Phys.* **67,** 1752 (1977).
4. P. P. Man, *J. Magn. Reson.* **94,** 258 (1991).
5. M. Bloom, J. H. Davis, and M. J. Valic, *Can. J. Phys.* **58,** 1510 (1980).
6. C. S. Choi, H. J. Prask, and E. Prince, *J. Chem. Phys.* **61,** 3523 (1974).
7. T. J. Bastow and S. N. Stuart, *J. Phys. Condens. Matter* **1,** 4649 (1989).